Journal of Quantitative Spectroscopy & Radiative Transfer 235 (2019) 300–308

Contents lists available at ScienceDirect

Journal of Quantitative Spectroscopy & Radiative Transfer

journal homepage: www.elsevier.com/locate/jqsrt

Extension of the discrete sources method to investigate the non-local effect influence on non-spherical core-shell particles

Yuri Eremin [a], Adrian Doicu [b], Thomas Wriedt [c,*]

[a] Lomonosov Moscow State University, Lenin's Hills, Moscow 119991, Russia
[b] Remote Sensing Technology Institute, German Aerospace Centre (DLR), Oberpfaffenhofen, Germany
[c] Leibniz-Institut für Werkstofforientierte Technologien - IWT, University of Bremen, Bremen, Germany

ARTICLE INFO

Article history:
Received 11 March 2019
Revised 10 July 2019
Accepted 10 July 2019
Available online 11 July 2019

Keywords:
Plasmonics
Non-local effect
SPASER resonator
Core-shell particles
Discrete
Sources method

ABSTRACT

The Discrete Sources Method (DSM) has been extended to model non-spherical, axisymmetric core-shell particles by taking into account the Non-local Effect (NLE). For this purpose, the Generalized Non-local Optical Response (GNOR) model of the NLE has been employed. By using the extended DSM numerical scheme, prolate and oblate core-shell spheroidal particles have been examined. The simulation results show that the influence of the NLE on both the far and the near field properties of plasmonic core-shell particles is essential. In particular it has been found that the plasmon resonance amplitude is decreased by about 40%, the near field intensity is reduced up to one order of a magnitude, and the blue shift of the plasmon resonance can reach value of 15 nm. Besides, it has been demonstrated that a larger shell refractive index leads to a higher value of the plasmon resonance.

1. Introduction

The optical properties of surface plasmons have been very successfully described in recent years within the framework of classical electromagnetic approaches that consider the dynamics of valence electrons in a metal as aggregate harmonic fluctuation of the electron charge density, whose behavior can be described by a classical polarizability. The electromagnetic fields associated with this collective movement of electrons are then analyzed based on the classic Maxwell's equations. This description assumes classical behavior of both electrons and electromagnetic fields to consider the electromagnetic properties of the near and far fields of metallic nanostructures, operating as optical nanoantennas [1,2]. Surface plasmons make it possible to confine the electromagnetic fields to subwavelength scale, which exceeds the conventional limit of optical diffraction. Plasmons, which refer to the hybridization between surface charges and electromagnetic fields, have catalyzed the emerging subject of plasmonics as an independent part of nanophotonics [3–5]. Due to this development, it became possible to obtain ultrahigh field enhancement and subwavelength field confinement far beyond the diffraction limit.

The metal nanoshell was first made in the latter 90s and since that time various structures of shells of increasing complexity have been obtained [6]. Such structures provide a greater flexibility in tuning plasmon resonances, as well as in realizing the needed amplification of electromagnetic fields. Core-shell nanoparticles have attracted increasing research interest due to their outstanding properties: [7]: (1) Versatility: a core-shell nanoparticle consists of an inner core and an outer shell made of different material; therefore, the combination of different properties of different materials leads to several novel properties, thus expanding their application; (2) Tunability: the properties of core-shell nanoparticles can be easily and dramatically tuned by changing the size, shape, morphology, and components of the core, as well as the thickness, shape, and material of the shell; (3) Stability and dispersibility: the coated shell can protect the nanoparticles from aggregation, sintering, or the effect of other reagents; (4) Biocompatibility: the biocompatibility is one of the important issues from the perspective of practical bioapplication, and the biocompatibility of nanoparticles can be improved by coating with silica (SiO_2), polymer, etc. Multilayered structures include, the "nanomatreshka" [8], which in the recent years attracted a great interest of researchers in the field of nanoplasmonics. In particular, core-shell particles constructed from composite nanomaterials have emerged as valuable nanomaterials for imaging and therapy [9], energy storage and conversion [10], photothermal enhancement [11], solar cell elements [12], SERS [8] and cloaking [13], owing to their complementary enhanced properties compared to their homogeneous counterparts. Among others, the most interest has been focused on cylindrical and spherical nanostructures due to the simplicity

* Corresponding author.
E-mail address: thw@iwt.uni-bremen.de (T. Wriedt).

https://doi.org/10.1016/j.jqsrt.2019.07.012
0022-4073/

of their geometry for a detailed theoretical investigation. Although the optical properties of these new plasmon structures are intriguing, the main attention was paid to the theoretical study of its spectral far field properties especially such characteristics as absorption cross-section, scattering and extinction. It is well known that due to the small size of these structures compared to the incident optical wavelength, the dipole approximation for the fields seem to be sufficient to describe scattering in the far zone, which makes theoretical study relatively simple. However, there are some optical phenomena, such as molecular fluorescence observed near these nanostructures, or catalysis [14] and photothermal enhancement [11], which are related to the near field of the structures. In these cases, more advanced theoretical approaches are required to describe all occurring physical processes.

Another important fundamental scientific problem within the framework of quantum plasmonics is the problem of creating nanoscale sources of coherent radiation. A fundamentally new approach seems to be using plasmon fields instead of photon fields. In fact plasmon fields allow to overcome the diffraction limitation in the size of a laser. A plasmonic nanolaser is called: SPASER (Surface Plasmon Amplification by Simulated Emission of Radiation) [15–17]. The concept of the spaser was first proposed by Stockman and Bergman in 2003 [18]. A spaser consists of nanoparticles of a noble metal, acting as nanoresonators, and an amplifying medium formed by resonantly coupled emitters [19]. In the first experimental implementation of the spaser, a core-shell nanostructure consisting of a gold nanosphere D = 14 nm with a SiO_2 spherical shell with an outer diameter of 44 nm doped with a laser dye was used [20]. Until now, a real laser consisting of noble metal nanostructures has not been experimentally implemented, although remarkable studies were devoted to the development of various promising nanoscale 3D structures of core-shell or core-metal type [16,21,22].

A laser resonator is a combination of an optical element that creates the spatial and spectral modes for photons. Similarly, a plasmon nanolaser resonator is a set of metal-dielectric nanostructures that form spatial and spectral modes for plasmons. An essential difference and advantage of a plasmon nanolaser compared to other existing sources of localized fields is that the plasmon nanolaser can operate in the regime, that is only weakly coupled to electromagnetic fields in the far zone. In other words, the plasmon nanolaser generates coherent, strongly localized near fields. This seems to be a considerable technological advantage. There exists two types of plasmons: localized surface plasmons and surface plasmon polaritons. These two types of plasmons are generated in a plasmon nanolaser using different types of resonators. There are three types of plasmon resonators: a 3D resonator for localized surface plasmons and 2D and 1D resonators for surface plasmon polaritons [23]. The most thoroughly studied type of 3D resonator is the nano-shell structure, which is one of the most promising geometric forms of nanostructures for a spaser [24]. The active medium in such a hybrid structure can be located both in the inner and outer regions of the nano-shell. In between non-spherical nanoparticles used as 3D resonators the more studied and frequently used are nanorods [22]. Elongated particles provide simple control of the center frequency of the plasmon resonance (PR) by changing the length of the particles, thereby adjusting the frequency of the PR of the nanoparticle to the required condition of the resonator [25].

The study of the quantum nature of electrons in metals and their collective optical response has a long tradition in condensed matter physics. Accounting for the influence of surfaces adds an additional degree of complexity, which requires special methods of solid state physics to adequately describe quantum interactions and the dynamics of electrons under the influence of external fields. In this context, the surface response of the electron gas was considered within the framework of various quantum approaches, including different quasiclassical hydrodynamic models [26,27], as well as methods based on time dependent density functional theory (TDDFT) [28]. The latter allows for a proper quantization of electrons which captures important aspects in plasmonics, such as the quantum size effect, dynamic screening of the electron gas, and the possibility of electron tunneling at optical frequencies [29]. Consideration of all these quantum effects provides a critical understanding of the fundamental limits of localization and field amplification in plasmonics, as well as the correct description of optoelectronic properties in metal nanoconstructions.

As a rule, for particle sizes smaller than 10 nm, a complete quantum mechanical description is required. For example, the TDDFT, which describes the collective motion of electrons, simulating the behavior of each electron, works well for explaining the experimental results for particle sizes of several nanometers [28]. As the size of plasmonic structures becomes less than the mean free path of the excited electrons, collisions between electrons cannot be neglected. Therefore, the motion of the conductive electrons is related not only to the field applied at the local position, but also depends on the fields at other positions. This defines the appearance of the non-local effect. To describe the optical properties of metal nanoparticles, various treatments accounting for quantum effects but within the framework of classical electromagnetic theory, also known as semi-classical approaches, have been developed [30,31]. For example, one such semiclassical method that takes into account non-local effects is the non-local hydrodynamic model, which takes into account the presence of longitudinal electric fields inside nanoparticles [32,33].

For the size-dependent plasmon damping, a geometry-dependent dielectric function is usually adopted [34], where the damping frequency in the Hydrodynamic Drude Model (HDM) is corrected according to the reduced mean free path of electrons. Alternatively, by simply correcting the nonlocal parameter by incorporation of a diffusion constant, the HDM has been extended to the Generalized Nonlocal Optical Response (GNOR) model [35]. In the frame of GNOR, size-dependent plasmon damping appears naturally via an additional constituent of the hydrodynamic description of induced charges in the metal, namely electron diffusion. GNOR has recently achieved considerable success in the areas of nanophotonics and nanoplasmonics [36–38]. GNOR has proven particularly efficient in recent years in simultaneously describing both nonlocal screening and Landau damping through a relatively simple correction of the wave equation that is straightforward to be implemented to any plasmonic geometry model [30,39]. Besides, GNOR has been completely justified by matching with TDDFT results [40] and comparison with experimental measurements [41]. We would like also to mention some publications in which the analysis of the optical properties of core-shell particles was investigated taking into account the non-local effect. However, in all these papers, researchers restricted to the consideration of spherical surfaces [42–44].

In this paper we will employ an extension of the discrete sources method. The DSM is a semi-analytical surface based meshless method. In the frame of DSM, the electromagnetic fields are constructed as finite linear combinations of discrete sources (DS) fields analytically satisfying the Maxwell equations in each domain and additionally the radiation conditions at infinity. The DS amplitudes are determined from the transmission conditions enforced at the interfaces of the media discontinuities. Compared to other surface based approaches, the DSM has some preferences: (I) it does not require any mesh generation or an integration procedure over the interfaces, (II) it provides the near and far fields in clear analytical form, (III) it simultaneously solves the scattering problem for all external excitations and polarizations at once, (IV) it can handle media with high refractive indices, and (V) it allows the estimation of the computational errors via estimation of the residual of the

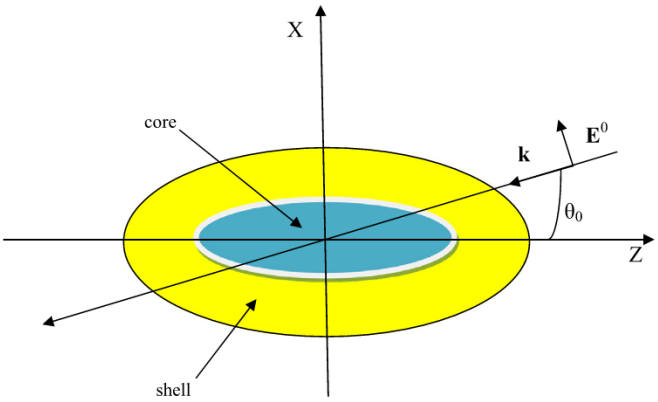

Fig. 1. Scattering geometry of a core-shell particles.

surface fields, which enables a near field computation with guaranteed accuracy [45]. These theoretical and numerical advantages recommend the discrete sources method for analyzing plasmonic structures in the presence of nonlocal response [46,47]. A detailed description of the numerical methods used in plasmonics can be found in the paper by Eremin et al. [47].

In this paper we present an extended scheme of the DSM that enables to analyze polarized light excitation of axial symmetric non-spherical core-shell plasmonic particles. For demonstration we choose the geometrical model of 3D spaser resonator consisting of a purely dielectric shell and a plasmonic core accounting for GNOR inside. This choice is due to the fact that for a 3D resonator it is important to provide near field amplification. The paper is organized as follows. In Section 2 we summarize the generalized nonlocal optical response model, and formulate the mathematical statement of the transmission boundary value scattering problem for the core-shell particle. Section 3 is devoted to the detailed description of the extended scheme of the discrete sources method, while in Section 4, computer-simulated results are reported and discussed.

2. Generalized nonlocal optical response model

Let us consider scattering of an electromagnetic plane wave ($\mathbf{E}^0$, $\mathbf{H}^0$) by an axisymmetric core-shell particle placed in an isotropic homogeneous medium as shown in Fig. 1. The particle consists of a metal core occupying the domain D_c with a smooth boundary ∂D_c, and a dielectric shell occupying the domain D_s with a smooth boundary ∂D_s. By assumption, all media are nonmagnetic and the surfaces $\partial D_{c,s}$ have a common axis of symmetry Oz. The incident electromagnetic plane wave propagates in the Oxz plane and along a direction which encloses the angle $\pi - \theta_0$ with the Oz axis.

Referring to the GNOR model, the following statements are relevant for our further analysis:

1. The local-response Ohm's law $\mathbf{J}(\mathbf{r}) = \sigma \mathbf{E}(\mathbf{r})$ is corrected for non-local response as [48]

$$\frac{\xi^2}{\varepsilon_b}\nabla[\nabla \cdot \mathbf{J}(\mathbf{r})] + \mathbf{J}(\mathbf{r}) = \sigma \mathbf{E}(\mathbf{r}), \tag{1}$$

where for the time dependence of the fields $\exp(\mathrm{j}\omega t)$,

$$\xi^2 = \varepsilon_b\left[\frac{\beta^2}{\omega(\omega - \mathrm{j}\gamma)} + \mathrm{j}\frac{D}{\omega}\right] \tag{2}$$

is the length scale of the GNOR model, ε_b the permittivity associated to bound charges, ω the exciting frequency, $\beta^2 = (3/5)v_F^2$, v_F the Fermi velocity, γ the Drude damping rate, D the diffusion constant, and σ the Drude conductivity.

2. The Maxwell equation for the magnetic field inside a metal core is

$$\nabla \times \mathbf{H}(\mathbf{r}) = \mathrm{j}\omega\varepsilon_0[\varepsilon_c + \xi^2\nabla(\nabla\cdot)]\mathbf{E}(\mathbf{r}), \tag{3}$$

where

$$\varepsilon_c = \varepsilon_b - \frac{\omega_p^2}{\omega^2 - \mathrm{j}\gamma\omega} \tag{4}$$

is the Drude permittivity, ε_0 the permittivity in vacuum, and ω_p the plasma frequency of the metal.

3. The field inside the metal core $\mathbf{E}$ consists of the contributions of a divergence-free transverse field $\mathbf{E}_T$, $\nabla \cdot \mathbf{E}_T = 0$ and a curl-free longitudinal field $\mathbf{E}_L$, $\nabla \times \mathbf{E}_L = 0$ solving the vector Helmholtz equation with the corresponding wavenumbers $k_T^2 = k_0^2\varepsilon_c$ and $k_L^2 = \varepsilon_c/\xi^2$, respectively, where $k_0 = \omega\sqrt{\varepsilon_0\mu_0}$ is the wavenumber in vacuum.

4. The amplitude of the longitudinal wave is computed from the additional boundary condition [47]

$$\varepsilon_b\widehat{\mathbf{n}}_c \cdot \mathbf{E}_c = \varepsilon_s\widehat{\mathbf{n}}_c \cdot \mathbf{E}_s, \tag{5}$$

which is imposed at the interface ∂D_c separating the metallic core D_c and the dielectric shell D_s. Here, $\widehat{\mathbf{n}}_c$ is the outward normal unit vector to the surface ∂D_c, and ε_s is the relative permittivity of the dielectric shell. The additional boundary condition is used together with the conventional boundary conditions namely, the continuity of the tangential components of the electric and magnetic fields at the corresponding interfaces.

Considering the scattering problem illustrated in Fig. 1, we are faced with the solution of the following boundary value scattering problem: Given the incident electromagnetic field ($\mathbf{E}^0$, $\mathbf{H}^0$), compute the scattered field ($\mathbf{E}_e, \mathbf{H}_e$) in $D_e = \mathbb{R}^3 \setminus \overline{D_c \cup D_s}$ and the internal fields ($\mathbf{E}_{c,s}, \mathbf{H}_{c,s}$) in $D_{c,s}$, satisfying the Maxwell equations

$$\nabla \times \mathbf{H}_{s,e} = \mathrm{j}k_0\varepsilon_{s,e}\mathbf{E}_{s,e}, \quad \nabla \times \mathbf{E}_{s,e} = -\mathrm{j}k_0\mathbf{H}_{s,e} \text{ in } D_{s,e} \tag{6}$$

$$\nabla \times \mathbf{H}_c = \mathrm{j}k_0[\varepsilon_c + \xi^2\nabla(\nabla\cdot)]\mathbf{E}_c, \quad \nabla \times \mathbf{E}_c = -\mathrm{j}k_0\mathbf{H}_c \text{ in } D_c \tag{7}$$

and the transmission conditions for the fields

$$\left.\begin{array}{c}\widehat{\mathbf{n}}_c \times (\mathbf{E}_c - \mathbf{E}_s) = 0, \ \widehat{\mathbf{n}}_c \times (\mathbf{H}_c - \mathbf{H}_s) = 0, \\ \varepsilon_b\widehat{\mathbf{n}}_c \cdot \mathbf{E}_c = \varepsilon_s\widehat{\mathbf{n}}_c \cdot \mathbf{E}_s \text{ on } \partial D_c,\end{array}\right| \tag{8}$$

and

$$\widehat{\mathbf{n}}_s \times (\mathbf{E}_s - \mathbf{E}_e) = \widehat{\mathbf{n}}_s \times \mathbf{E}^0, \ \widehat{\mathbf{n}}_s \times (\mathbf{H}_s - \mathbf{H}_e) = \widehat{\mathbf{n}}_s \times \mathbf{H}^0 \text{ on } \partial D_s. \tag{9}$$

In addition, the scattered field must satisfy the Silver-Müller radiation condition at infinity. Here, ε_e is the relative permittivity of the ambient dielectric medium, and $\widehat{\mathbf{n}}_s$ is outward normal unit vector to the surface ∂D_s.

Note that the field inside the core is decomposed as

$$\mathbf{E}_c = \mathbf{E}_{Tc} + \mathbf{E}_{Lc}, \tag{10}$$

where $\mathbf{E}_{Tc}$ and $\mathbf{E}_{Lc}$ are the transverse and longitudinal fields, satisfying

$$\nabla \cdot \mathbf{E}_{Tc} = 0 \text{ and } \nabla \times \mathbf{E}_{Lc} = 0.$$

3. Extended scheme of the discrete sources method

In the framework of the discrete sources method, the electromagnetic fields are constructed as finite linear combinations of the fields produced by dipoles and multipoles distributed inside the core-shell particle. Thus, the solution satisfies the Maxwell equations and the radiation condition at infinity. The unknown amplitudes of the discrete sources are determined from the transmission

conditions enforced at the interfaces ∂D_c and ∂D_s. In this section we describe an extended scheme of the discrete sources method for modeling the nonlocal optical response for a core-shell particle.

For the incident electromagnetic plane wave

$$\mathbf{E}_0(\mathbf{r}) = \widehat{\mathbf{e}}_0 e^{-j\mathbf{k}_e\cdot\mathbf{r}} \tag{11}$$

propagating along the direction $(\pi-\theta_0,\pi)$ and being characterized by the wave vector $\mathbf{k}_e = k_e\widehat{\mathbf{k}}_e$, $k_e = k_0\sqrt{\varepsilon_e}$ and the polarization unit vector $\widehat{\mathbf{e}}_0$, the corresponding P- and S-polarized incident fields are given respectively, by

$$\mathbf{E}^{0P}(\mathbf{r}) = (\cos\theta_0\widehat{\mathbf{e}}_x + \sin\theta_0\widehat{\mathbf{e}}_z)\cdot\chi(x,z), \tag{12}$$

$$\mathbf{H}^{0P}(\mathbf{r}) = -\sqrt{\varepsilon_e}\widehat{\mathbf{e}}_y\cdot\chi(x,z), \tag{13}$$

and

$$\mathbf{E}^{0S}(\mathbf{r}) = \widehat{\mathbf{e}}_y\cdot\chi(x,z), \tag{14}$$

$$\mathbf{H}^{0S}(\mathbf{r}) = \sqrt{\varepsilon_e}(\cos\theta_0\widehat{\mathbf{e}}_x + \sin\theta_0\widehat{\mathbf{e}}_z)\cdot\chi(x,z), \tag{15}$$

where $(\widehat{\mathbf{e}}_x,\widehat{\mathbf{e}}_y,\widehat{\mathbf{e}}_z)$ are the Cartesian unit vectors and

$$\chi(x,z) = e^{-jk_e(x\sin\theta_0 - z\cos\theta_0)}. \tag{16}$$

For an axisymmetric particle, the P- and S-polarized excitations are treated separately [45]. To account for axial symmetry, we expand each polarized plane wave into a Fourier series in the azimuthal angle φ by using the relation

$$e^{\pm jx\cos\varphi} = \sum_{m=0}^{\infty}(2-\delta_{m0})(\pm j)^m J_m(x)\cos m\varphi, \tag{17}$$

where J_m are the cylindrical Bessel functions, and δ_{m0} is the Kronecker delta symbol. The scattering problem then decouples over the azimuthal modes m, and a separate solution for each m is obtained.

The discrete sources are distributed along the axis Oz (the axis of symmetry of the core-shell particle), and in this regard, we denote by $\{z_n^e\}_{n=1}^{N_e^m}$ the positions of the discrete sources for representing the scattered field, by $\{z_n^s\}_{n=1}^{N_s^m}$ the positions of the discrete sources for representing the field inside the dielectric shell, by $\{z_n^{Tc}\}_{n=1}^{N_{Tc}^m}$ the positions of the discrete sources for representing the transverse field inside the metal core, and finally, by $\{z_n^{Lc}\}_{n=1}^{N_{Lc}^m}$ the positions of the discrete sources for representing the longitudinal field inside the core. Note that the numbers of discrete sources N_e^m, N_s^m, N_{Tc}^m and N_{Lc}^m may depend on the azimuthal mode order m. It is important to mention that the field inside the shell is represented as a superposition of incoming and outgoing waves.

For approximation of the transverse fields, the fields of the discrete sources are constructed from the vector potentials

$$\begin{aligned}\mathbf{A}_{mn}^{1\alpha}(\mathbf{r}) &= Y_m^\alpha(\boldsymbol{\varrho},z_n^\alpha)\cos[(m+1)\varphi]\widehat{\mathbf{e}}_\rho \\ &\quad - Y_m^\alpha(\boldsymbol{\varrho},z_n^\alpha)\sin[(m+1)\varphi]\widehat{\mathbf{e}}_\varphi,\end{aligned} \tag{18}$$

$$\begin{aligned}\mathbf{A}_{mn}^{2\alpha}(\mathbf{r}) &= Y_m^\alpha(\boldsymbol{\varrho},z_n^\alpha)\sin[(m+1)\varphi]\widehat{\mathbf{e}}_\rho \\ &\quad + Y_m^\alpha(\boldsymbol{\varrho},z_n^\alpha)\cos[(m+1)\varphi]\widehat{\mathbf{e}}_\varphi,\end{aligned} \tag{19}$$

$$\mathbf{A}_{mn}^{3\alpha}(\mathbf{r}) = Y_0^\alpha(\boldsymbol{\varrho},z_n^\alpha)\widehat{\mathbf{e}}_z,\ \alpha = \mathrm{e},\mathrm{c},\mathrm{s}\pm. \tag{20}$$

where

$$Y_m^c(\boldsymbol{\varrho},z_n^c) = j_m(k_cR_{z_n^c})\left(\frac{\rho}{R_{z_n^c}}\right)^m, \tag{21}$$

$$Y_m^e(\boldsymbol{\varrho},z_n^e) = h_m^{(2)}(k_eR_{z_n^e})\left(\frac{\rho}{R_{z_n^e}}\right)^m, \tag{22}$$

$$Y_m^{s\pm}(\boldsymbol{\varrho},z_n^s) = h_m^{(2,1)}(k_sR_{z_n^s})\left(\frac{\rho}{R_{z_n^s}}\right)^m, \tag{23}$$

the plus sign corresponds to the outgoing waves $h_m^{(2)}$, the minus sign corresponds to the incoming waves $h_m^{(1)}$, $k_{c,s} = k_0\sqrt{\varepsilon_{c,s}}$, $\boldsymbol{\varrho} = (\rho,z)$, $\rho^2 = x^2+y^2$, and

$$R_{z_n}^2 = \rho^2 + (z-z_n)^2. \tag{24}$$

Here we would like to emphasize that we use Hankel functions of 1st and 2nd kinds $h_m^{(2,1)}$ instead of Bessel and Neuman functions which is a common choice for the core-shell particle [43].

For approximation of longitudinal fields, the fields of the discrete sources are constructed from the scalar potentials Ψ_{mn} and Ψ_n as given below. So, for a P-polarized excitation, the approximate solution is given by

$$\begin{aligned}\mathbf{E}_{T\alpha}^{\mathcal{N}}(\mathbf{r}) &= \sum_{m=0}^{M}\sum_{n=1}^{N_\alpha^m} p_{mn}^{T\alpha}\frac{j}{k_0\varepsilon_\alpha}\nabla\times\nabla\times\mathbf{A}_{mn}^{1\alpha}(\mathbf{r}) + q_{mn}^{T\alpha}\frac{j}{\varepsilon_\alpha}\nabla\times\mathbf{A}_{mn}^{2\alpha}(\mathbf{r}) \\ &\quad + \sum_{n=1}^{N_\alpha^0} r_n^{T\alpha}\frac{j}{k_0\varepsilon_\alpha}\nabla\times\nabla\times\mathbf{A}_n^{3\alpha}(\mathbf{r}),\quad \alpha = \mathrm{c},\mathrm{e},\mathrm{s}\pm,\end{aligned} \tag{25}$$

$$\mathbf{E}_{Lc}^{\mathcal{N}}(\mathbf{r}) = \sum_{m=0}^{M}\sum_{n=1}^{N_{Lc}^m} p_{mn}^{Lc}\nabla\Psi_{mn}(\mathbf{r}) + \sum_{n=1}^{N_{Lc}^0} r_n^{Lc}\nabla\Psi_n(\mathbf{r}), \tag{26}$$

$$\mathbf{H}_\alpha^{\mathcal{N}}(\mathbf{r}) = \frac{j}{k_0}\nabla\times\mathbf{E}_\alpha^{\mathcal{N}}(\mathbf{r}), \tag{27}$$

where the scalar potentials Ψ_{mn} and Ψ_n are defined as

$$\Psi_{mn}(\mathbf{r}) = j_m(k_LR_{z_n^{Lc}})\left(\frac{\rho}{R_{z_n^{Lc}}}\right)^{m+1}\cos[(m+1)\varphi], \tag{28}$$

$$\Psi_n(\mathbf{r}) = j_0(k_LR_{z_n^{Lc}}), \tag{29}$$

$k_L^2 = \varepsilon_c/\xi^2$, and M is the maximum number of azimuthal modes. For an S-polarized excitation, we have

$$\begin{aligned}\mathbf{E}_{T\alpha}^{\mathcal{N}}(\mathbf{r}) &= \sum_{m=0}^{M}\sum_{n=1}^{N_\alpha^m} p_{mn}^{T\alpha}\frac{j}{k_0\varepsilon_\alpha}\nabla\times\nabla\times\mathbf{A}_{mn}^{2\alpha}(\mathbf{r}) + q_{mn}^{T\alpha}\frac{j}{\varepsilon_\alpha}\nabla\times\mathbf{A}_{mn}^{1\alpha}(\mathbf{r}) \\ &\quad + \sum_{n=1}^{N_\alpha^0} r_n^{T\alpha}\frac{j}{\varepsilon_\alpha}\nabla\times\mathbf{A}_n^{3\alpha}(\mathbf{r}),\quad \alpha = \mathrm{c},\mathrm{e},\mathrm{s}\pm,\end{aligned} \tag{30}$$

$$\mathbf{E}_{Lc}^{\mathcal{N}}(\mathbf{r}) = \sum_{m=0}^{M}\sum_{n=1}^{N_{Lc}^m} p_{mn}^{Lc}\nabla\Psi_{mn}(\mathbf{r}), \tag{31}$$

$$\mathbf{H}_\alpha^{\mathcal{N}}(\mathbf{r}) = \frac{j}{k_0}\nabla\times\mathbf{E}_\alpha^{\mathcal{N}}(\mathbf{r}), \tag{32}$$

where the scalar potentials Ψ_{mn} are now defined by

$$\Psi_{mn}(\mathbf{r}) = j_m(k_LR_{z_n^{Lc}})\left(\frac{\rho}{R_{z_n^{Lc}}}\right)^{m+1}\sin[(m+1)\varphi]. \tag{33}$$

Note that the basis functions $Y_m^\alpha(\boldsymbol{\varrho},z_n)$ and $\Psi_{mn}(\mathbf{r})$ are the so-called lowest-order distributed multipoles [49].

Some remarks are in order:

1. $\mathcal{N}$ is a multi-index incorporating both the maximum number of azimuthal modes M, and the number of discrete sources $N_{e,c,s\pm}^m$, N_{Tc}^m and N_{Lc}^m.

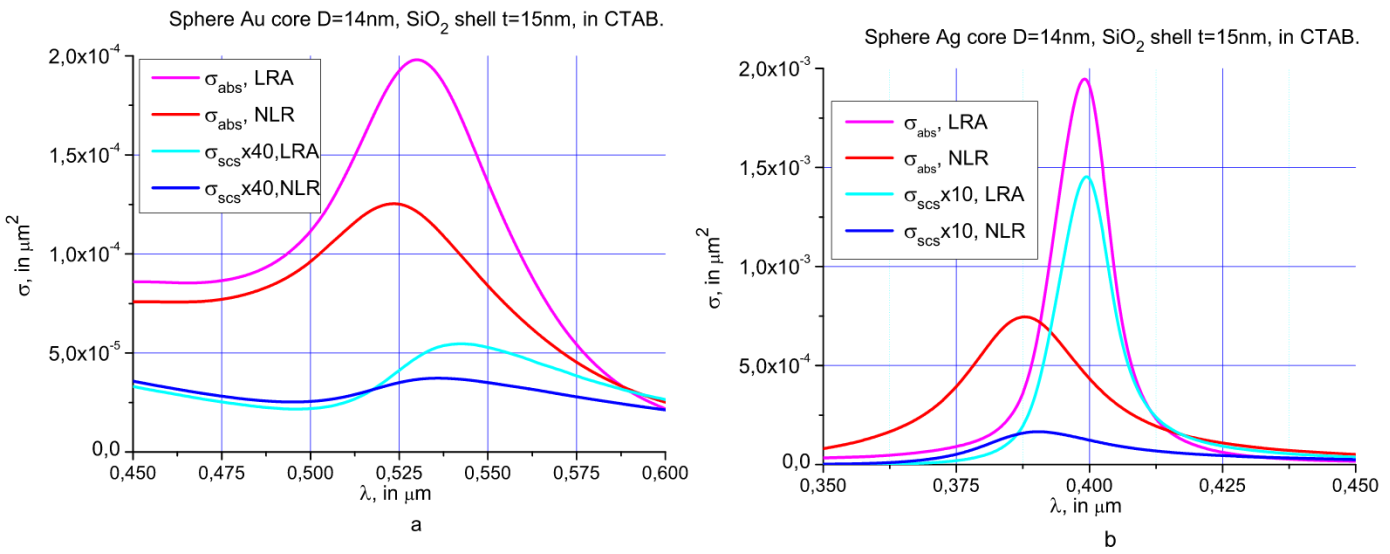

Fig. 2. Absorption and scattering cross sections computed by LRA and GNOR (NLR). The diameter of the spherical core is $D = 14$ nm, and the thickness of the SiO_2 shell is $t = 15$ nm. The results corresponding to the gold and silver cores are illustrated in the left (a) and right (b) panels, respectively.

2. From (27) and (32) it is apparent that only the transverse field **E** contributes to the magnetic field **H** inside the metallic core of the particle.
3. In the case of an S-polarized excitation, the azimuthal independent harmonic does not contain the nonlocal term $\nabla\Psi_n$ appearing in (26). The reason for this is that in this case, there is no normal component of the electric field, and so, the additional boundary condition is not required.

As the electromagnetic fields given by (25)–(27) and (30)–(32) solve the Maxwell Eqs (6)–(7), we have to determine the amplitudes of DS

$$\{p_{mn}^{\mathrm{T}\alpha},\ q_{mn}^{\mathrm{T}\alpha},\ r_{n}^{\mathrm{T}\alpha},\ p_{mn}^{\mathrm{Lc}},\ r_{n}^{\mathrm{Lc}}\},\alpha = \mathrm{e},\mathrm{c},\mathrm{s}\pm$$

such that the boundary conditions (8)–(9) are fulfilled. By means of the generalized point matching technique, we obtain the following relations for computing the amplitudes of the discrete sources:

$$\widehat{\mathbf{n}}_{\mathrm{c}} \times \int_0^{2\pi} [\mathbf{E}_{\mathrm{Tc}}^N(\boldsymbol{\rho}_l,\varphi) + \mathbf{E}_{\mathrm{Lc}}^N(\boldsymbol{\rho}_l,\varphi) - \mathbf{E}_{\mathrm{s}}^N(\boldsymbol{\rho}_l,\varphi)]\mathrm{e}^{-\mathrm{j}m\varphi}\mathrm{d}\varphi = 0, \quad (34)$$

$$\widehat{\mathbf{n}}_{\mathrm{c}} \times \int_0^{2\pi} [\mathbf{H}_{\mathrm{c}}^N(\boldsymbol{\rho}_l,\varphi) - \mathbf{H}_{\mathrm{s}}^N(\boldsymbol{\rho}_l,\varphi)]\mathrm{e}^{-\mathrm{j}m\varphi}\mathrm{d}\varphi = 0, \quad (35)$$

$$\widehat{\mathbf{n}}_{\mathrm{c}} \cdot \int_0^{2\pi} [\varepsilon_{\mathrm{b}}\mathbf{E}_{\mathrm{Ts}}^N(\boldsymbol{\rho}_l,\varphi) + \varepsilon_{\mathrm{b}}\mathbf{E}_{\mathrm{Ls}}^N(\boldsymbol{\rho}_l,\varphi) - \varepsilon_{\mathrm{s}}\mathbf{E}_{\mathrm{s}}^N(\boldsymbol{\rho}_l,\varphi)]\mathrm{e}^{-\mathrm{j}m\varphi}\mathrm{d}\varphi = 0, \quad (36)$$

$$\widehat{\mathbf{n}}_{\mathrm{s}} \times \int_0^{2\pi} [\mathbf{E}_{\mathrm{s}}^N(\boldsymbol{\varrho}_l,\varphi) - \mathbf{E}_{\mathrm{e}}^N(\boldsymbol{\varrho}_l,\varphi)]\mathrm{e}^{-\mathrm{j}m\varphi}\mathrm{d}\varphi = \widehat{\mathbf{n}}_{\mathrm{s}} \times \int_0^{2\pi} \mathbf{E}^0(\boldsymbol{\varrho}_l,\varphi)\mathrm{e}^{-\mathrm{j}m\varphi}\mathrm{d}\varphi, \quad (37)$$

$$\widehat{\mathbf{n}}_{\mathrm{s}} \times \int_0^{2\pi} [\mathbf{H}_{\mathrm{s}}^N(\boldsymbol{\varrho}_l,\varphi) - \mathbf{H}_{\mathrm{e}}^N(\boldsymbol{\varrho}_l,\varphi)]\mathrm{e}^{-\mathrm{j}m\varphi}\mathrm{d}\varphi = \widehat{\mathbf{n}}_{\mathrm{s}} \times \int_0^{2\pi} \mathbf{H}^0(\boldsymbol{\varrho}_l,\varphi)\mathrm{e}^{-\mathrm{j}m\varphi}\mathrm{d}\varphi, \quad (38)$$

where $\{\boldsymbol{\varrho}_l\}_{l=1}^{L_{\mathrm{s}}}$, $\{\boldsymbol{\rho}_l\}_{l=1}^{L_{\mathrm{c}}}$ are the sets of matching points distributed in the azimuthal plane $\varphi = \mathtt{const}$ over the meridians of the surfaces $\partial D_{\mathrm{s,c}}$. Let us remind that inside the shell $\mathbf{E}_{\mathrm{s}}^N = \mathbf{E}_{\mathrm{s}+}^N + \mathbf{E}_{\mathrm{s}-}^N$ and $\mathbf{H}_{\mathrm{s}}^N = \mathbf{H}_{\mathrm{s}+}^N + \mathbf{H}_{\mathrm{s}-}^N$. For each order m, the numbers of DS and matching points are chosen such that

$$2N_{\mathrm{Tc}}^m + N_{\mathrm{Lc}}^m + 4N_{\mathrm{s}}^m + 2N_{\mathrm{e}}^m \le 5L_{\mathrm{c}} + 4L_{\mathrm{s}}, \quad (39)$$

in which case, we are led to an overdetermined system of equations for computing the amplitudes of the DS. This system of equations is solved in the least squares sense by using a QR matrix factorization for a given set of incident angles θ_0, and simultaneously for both P- and S-polarized excitation.

Once the amplitudes of the discrete sources are known, the components of the far-field pattern

$$\mathbf{F}(\theta,\varphi) = F_\theta(\theta,\varphi)\widehat{\mathbf{e}}_\vartheta + F_\varphi(\theta,\varphi)\widehat{\mathbf{e}}_\varphi, \quad (40)$$

defined through the relation [50]

$$\mathbf{E}_{\mathrm{e}}(\mathbf{r}) = \frac{\mathrm{e}^{-\mathrm{j}k_{\mathrm{e}}r}}{r}\mathbf{F}(\theta,\varphi) + o\left(\frac{1}{r}\right), \quad r \to \infty, \quad (41)$$

are computed for a P-polarized excitation as

$$F_\theta^{\mathrm{P}}(\theta,\varphi) = \mathrm{j}k_{\mathrm{e}}\sum_{m=0}^{M}(\mathrm{j}\sin\theta)^m\cos[(m+1)\varphi] \sum_{n=1}^{N_{\mathrm{e}}^m}(p_{mn}^{\mathrm{e}}\cos\theta + q_{mn}^{\mathrm{e}})\mathrm{e}^{-\mathrm{j}k_{\mathrm{e}}z_n^{\mathrm{e}}\cos\theta} - \mathrm{j}k_{\mathrm{e}}\sin\theta\sum_{n=1}^{N_{\mathrm{e}}^0} r_n^{\mathrm{e}}\mathrm{e}^{-\mathrm{j}k_{\mathrm{e}}z_n^{\mathrm{e}}\cos\theta}, \quad (42)$$

$$F_\varphi^{\mathrm{P}}(\theta,\varphi) = -\mathrm{j}k_{\mathrm{e}}\sum_{m=0}^{M}(\mathrm{j}\sin\theta)^m\sin[(m+1)\varphi] \sum_{n=1}^{N_{\mathrm{e}}^m}(p_{mn}^{\mathrm{e}} + q_{mn}^{\mathrm{e}}\cos\theta)\mathrm{e}^{-\mathrm{j}k_{\mathrm{e}}z_n^{\mathrm{e}}\cos\theta} \quad (43)$$

and for an S-polarized excitation as

$$F_\theta^{\mathrm{S}}(\theta,\varphi) = \mathrm{j}k_{\mathrm{e}}\sum_{m=0}^{M}(\mathrm{j}\sin\theta)^m\sin[(m+1)\varphi] \sum_{n=1}^{N_{\mathrm{e}}^m}(p_{mn}^{\mathrm{e}}\cos\theta - q_{mn}^{\mathrm{e}})\mathrm{e}^{-\mathrm{j}k_{\mathrm{e}}z_n^{\mathrm{e}}\cos\theta} \quad (44)$$

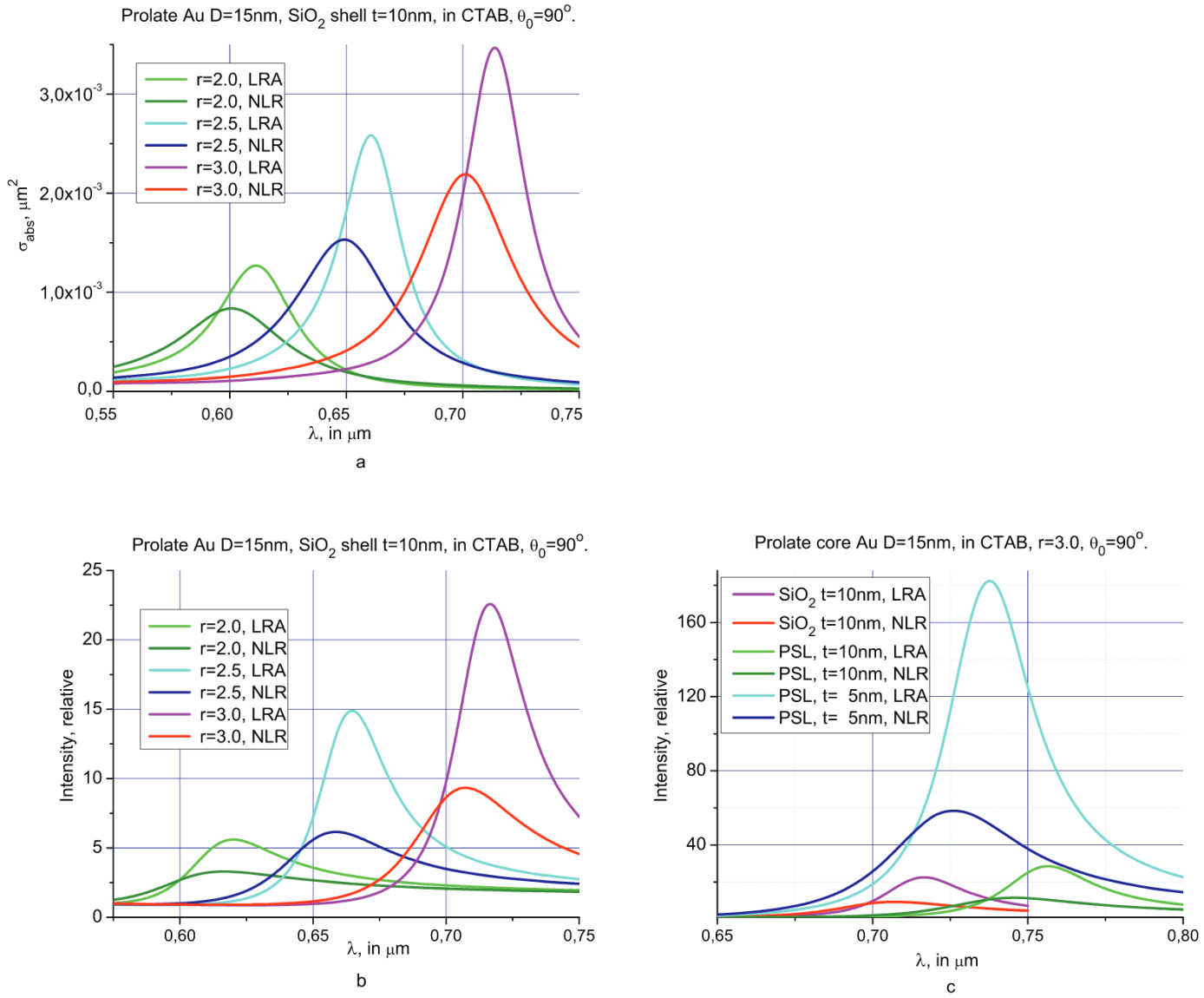

Fig. 3. Absorption cross section (a) and relative intensity computed by LRA and GNOR (NLR) (b,c). In (a) and (b), the core-shell particle is a prolate spheroid with a gold core, and a SiO_2 shell. The equivolumetric diameter is $D_c = 15$ nm, the shell thickness is $t = 10$ nm, and the aspect ratios are $r = 2.0, 2.5, 3.0$. In (c), the relative intensity corresponds to a SiO_2 and a PSL shell, the shell thicknesses are $t = 5, 10$ nm, and the aspect ratio is $r = 3.0$.

$$F_\varphi^{\mathrm{S}}(\theta,\varphi) = \mathrm{j}k_{\mathrm{e}} \sum_{m=0}^{M} (\mathrm{j}\sin\theta)^m \cos[(m+1)\varphi] \sum_{n=1}^{N_{\mathrm{e}}^m} (p_{mn}^{\mathrm{e}} \cos\theta - q_{mn}^{\mathrm{e}}) \mathrm{e}^{-\mathrm{j}k_{\mathrm{e}} z_n^{\mathrm{e}} \cos\theta} + \mathrm{j}k_{\mathrm{e}} \sin\theta \sum_{n=1}^{N_{\mathrm{e}}^0} r_n^{\mathrm{e}} \mathrm{e}^{-\mathrm{j}k_{\mathrm{e}} z_n^{\mathrm{e}} \cos\theta}. \tag{45}$$

The differential scattering cross section is then calculated as

$$\sigma^{\mathrm{P,S}}(\theta,\varphi) = |F_\theta^{\mathrm{P,S}}(\theta,\varphi)|^2 + |F_\varphi^{\mathrm{P,S}}(\theta,\varphi)|^2, \tag{46}$$

the scattering cross section as [51]

$$\sigma_{\mathrm{scs}}^{\mathrm{P,S}} = \int_0^{2\pi} \int_0^{\pi} \sigma^{\mathrm{P,S}}(\theta,\varphi) \sin\theta \, \mathrm{d}\theta \, \mathrm{d}\varphi, \tag{47}$$

and the extinction cross sections for P- and S-polarized excitations as

$$\sigma_{\mathrm{ext}}^{\mathrm{P}} = -\frac{4\pi}{k_{\mathrm{e}}} \mathrm{Im}[F_\theta^{\mathrm{P}}(\pi - \theta_0, \pi)] \tag{48}$$

and

$$\sigma_{\mathrm{ext}}^{\mathrm{S}} = \frac{4\pi}{k_{\mathrm{e}}} \mathrm{Im}[F_\varphi^{\mathrm{S}}(\pi - \theta_0, \pi)], \tag{49}$$

respectively. According to the optical theorem [51], the absorption cross-section can be then computed as $\sigma_{\mathrm{abs}} = \sigma_{\mathrm{ext}} - \sigma_{\mathrm{scs}}$. From (42)–(45) it is readily seen that the components of the far-field pattern are expressed through finite linear combinations of elementary functions, and so, that no integration procedure is required for their computation. Besides, the errors in the solution can be estimated by computing the residual norm of the boundary condition of the surface fields at the core and the shell interfaces $\partial D_{\mathrm{c,s}}$ [45].

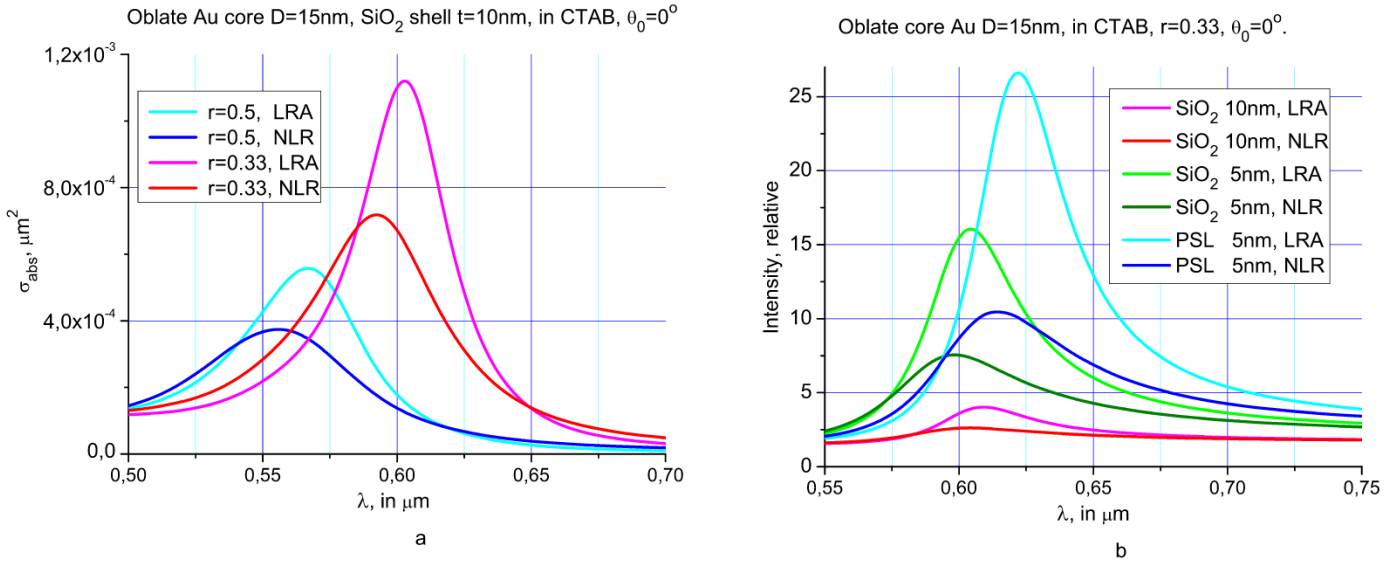

Fig. 4. Absorption cross section (a) and relative intensity computed by LRA and GNOR (NLR) (b), incident angle is $\theta_0 = 0^\circ$. In (a), the core-shell particle is an oblate spheroid with a gold core, and a SiO_2 shell. The equivolumetric diameter is $D_c = 15$ nm, the shell thickness is $t = 10$ nm, and the aspect ratios are $r = 0.5, 0.33$. In (b), the relative intensity corresponds to a SiO_2 and a PSL shell, the shell thicknesses are $t = 5, 10$ nm, and the aspect ratio is $r = 0.33$.

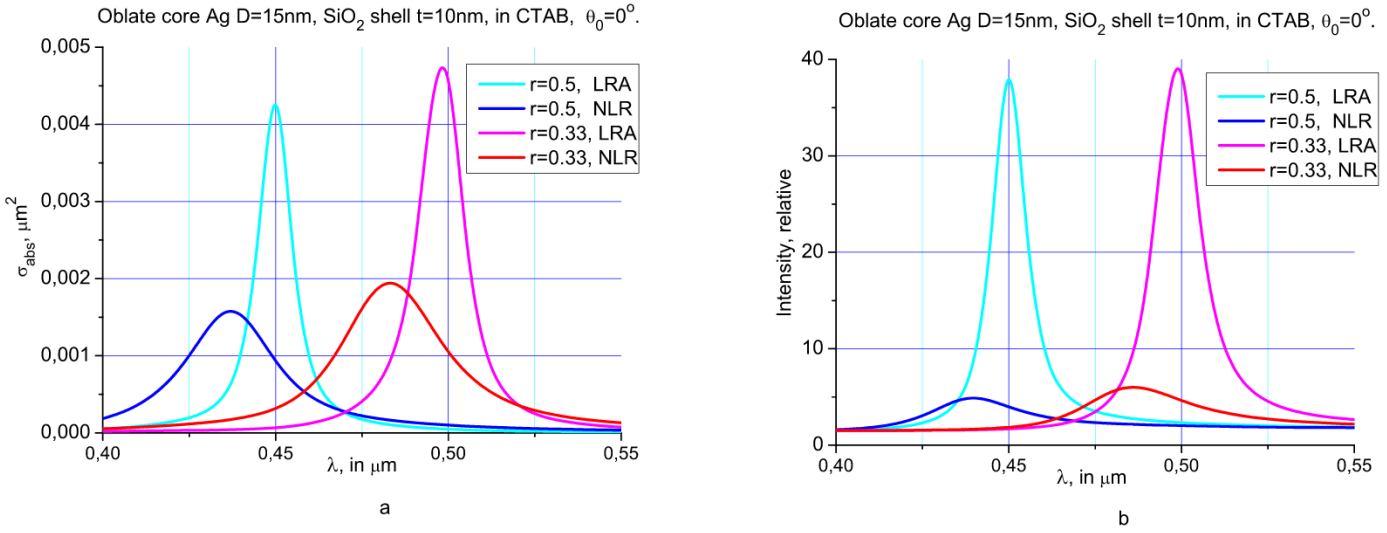

Fig. 5. The same as in Fig. 4 but for an oblate spheroid with a silver core.

4. Computer simulation results

In this section we consider the scattering of a plasmonic spheroidal core-shell particle, consisting of a metallic gold (Au) or silver (Ag) core and a dielectric silica SiO_2 ($n_s = 1.46$) or PSL (polystyrene latex) ($n_s = 1.6$) shell, placed in a hexadecyltrimethylammonium bromide (CTAB) background (ambient) medium with the refractive index $n_e = 1.336$ [17]. For gold and silver, the frequency dependent refractive index $n_c = \sqrt{\varepsilon_c}$ is taken from [52]. The corresponding GNOR parameters for Au have been chosen as [48]:

$$\hbar\omega_p = 9.02\,\text{eV},\quad \hbar\gamma = 0.071\,\text{eV},\quad v_F = 1.39\,\mu\text{m/s},\quad D = 8.62\cdot 10^8\,\mu\text{m}^2/s$$

and for Ag

$$\hbar\omega_p = 8.99\,\text{eV},\quad \hbar\gamma = 0.025\,\text{eV},\quad v_F = 1.39\,\mu\text{m/s},\quad D = 9.62\cdot 10^8\,\mu\text{m}^2/s$$

We start by considering a spherical core-shell resonator, which has been analyzed in multiple reviews [16] starting from Noginov paper (see Fig. 2 of [20]). Fig. 2a shows the absorption and scattering cross-sections computed with the local response (LRA) and nonlocal response (NLR) - GNOR models. It is apparent that the plasmon resonance amplitude decreases up to 40%, and that there is a small blue shift when the NLE is considered. A similar observation can be made for the scattering cross section. For a silver core, the corresponding results are illustrated in Fig. 2b. In this case, the PR damping exceeds 60% with a larger blue shift. It is clear that the corresponding silver curve seems to be blue shifted in comparison to the gold curve and that it is a bit sharper.

Next, we investigate the influence of the NLE on a nonspherical core-shell particle. For this purpose, we consider a prolate core-shell particle with the equivolumetric diameter $D_c = 15$nm, and the shell thickness $t = 10$nm [17,53]. The simulation results, corresponding to a gold core and the incidence angle $\theta_0 = 90^\circ$, are depicted in Fig. 3a. Note that for this incidence angle, the electric field vector $\mathbf{E}^0$ is parallel to the larger axis of the metallic core [47]. The results show a PR damping up to 40%, a blue shift of about

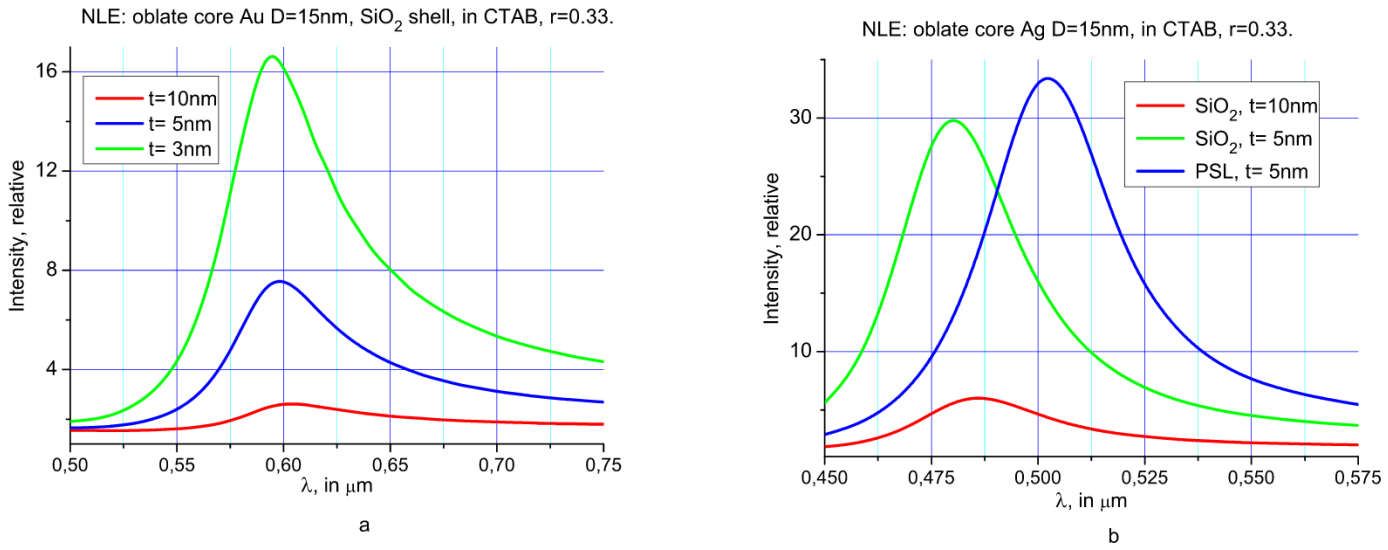

Fig. 6. Relative intensity computed by GNOR only. In (a), the core-shell particle is an oblate spheroid with a gold core, and a SiO_2 shell. The equivolumetric diameter is $D_c = 15$ nm, the shell thicknesses are $t = 3$, 5, 10 nm, and the aspect ratio is $r = 0.33$. In (b), the core-shell particle is an oblate spheroid with a silver core, the materials of the shell are SiO_2 and PSL, the equivolumetric diameter is $D_c = 15$ nm, the shell thicknesses are $t = 5$, 10 nm, and the aspect ratio is $r = 0.33$.

12 nm, and a plasmon resonance curve broadening. In Fig. 3b we plot the averaged relative intensity $\left|\mathbf{E_e} + \mathbf{E}^0\right|^2 / \left|\mathbf{E}^0\right|^2$ in the vicinity of the shell surface. The results are similar to those obtained in Fig. 3a. In Fig. 3c we analyzed the influence of the shell material and its thickness on the relative intensity for a gold core with an aspect ratio of $r = 3.0$. As it is clear, a PSL shell of smaller thickness, leads to an increase of the near field relative intensity of up to 60%. It is worth to mention that in a spaser model, the nanorods are usual randomly oriented with respect to the polarization of the exciting $\mathbf{E^0}$ [53] (see Fig. 1d). Because the P-polarized amplitude of the PR exceeds the S-polarized amplitudes by an order of magnitude, by averaging the relative intensity over the angle of polarization, it may happen that the PR amplitude decreases by 50%. For this reason, we repeat the previous simulations but for an oblate core-shell particle. The simulation results are shown in Fig. 4. In this case, the incidence angle is $\theta_0 = 0^\circ$ so that the larger axis of the metallic core is parallel to the $\mathbf{E}^0$ vector. The same features that we already observed for a prolate core-shell particle are visible.

The results in Fig. 5 correspond to a silver core [54]. In this case, the relative intensity decreases by almost one order of magnitude, the blue shift is about 15 nm, and there is a large broadening of the PR curve. The results in Fig. 6 demonstrate that a reduction of the shell thickness increases the relative intensity. Besides, a silver core provides higher intensity then a gold core but there is a resonance shift to shorter wavelength. In summary of our computer simulation, we can conclude that an oblate particle does not provide higher field enhancement as compared to a prolate particle.

Metal-dielectric nanoparticles can be used for multiple practical applications via their enhanced plasmon resonance due to stronger Coulombic interactions between polarization charges of the dielectric shell and the free electrons in the plasmonic core as a result of the dielectric shell having larger refractive index than the metal core [55]. That is probably the reason that a PSL shell demonstrates larger intensity peaks then a SiO_2 shell.

5. Conclusions

The Discrete Sources Method in conjunction with the GNOR model has been extended to analyze the influence of the non-local effect on the scattering and near field properties of non-spherical, core-shell particle. In particular, the absorption and the scattering cross sections, as well as the relative near field intensity for such kind of scatterers have been computed. The numerical results demonstrate the large influence of the non-local effect on both far field and near field properties of plasmonic nano-particles. We found that the plasmon resonance amplitude is decreased about 40%, the near field intensity is reduced up to one order of a magnitude, and the blue shift of the plasmon resonance can reach the value of 15 nm in case of the non-local effect accounting for. Besides, it has been demonstrated that larger shell refractive index leads to high value of the plasmon resonance.

Acknowledgment

This work was supported by the Deutsche Forschungsgemeinschaft (DFG) under grant WR 22/59-1.

References

[1] Tame MS, McEnery KR, Ozdemir SK, et al. Quantum plasmonics. Nat Phys 2013;9:329–40.
[2] Xu D, Xiong X, Wu L, et al. Quantum plasmonics: new opportunity in fundamental and applied photonics. Rev Adv Opt Photon 2018;10(4):703–56.
[3] Maier SA. Plasmonics: fundamentals and applications. Springer; 2007.
[4] Pelton M, Bryant G. Introduction to metal-nanoparticle plasmonics. John Wiley & Sons; 2013.
[5] Polman A, Atwater HA. Plasmonics: optics at the nanoscale. Mater Today 2005;8(1):56.
[6] Oldenburg SJ, Averitt RD, Westcott SL, Halas NJ. Nanoengineering of optical resonances. Chem Phys Lett 1998;288(2):243–7.
[7] J-F L, et al. Core-shell nanoparticle-enhanced raman spectroscopy. (review). Chem Rev 2017;117:5002–509.
[8] Lin L, Gu H, Ye J. Plasmonic multi-shell nanomatryoshka particles as highly tunable SERS tags with built-in reporters. Chem Commun 2015;51:17740–3.
[9] Moreira AF. Gold-core silica shell nanoparticles application in imaging and therapy: a review. Microporous Mesoporous Mater 2018;270:168–79.
[10] H-P F. Core-shell nanomaterials: applications in energy storage and conversion. Adv Colloid Interface Sci 2019;267:26–46.
[11] Phan AD, Nga DT, Viet NA. Theoretical model for plasmonic photothermal response of gold nanostructures solutions. Opt Commun 2018;410:108–11.
[12] Zhang W, Saliba M, Stranks SD, et al. Enhancement of perovskite-based solar cells employing core-shell metal nanoparticles. Nano Lett 2013;13:4505–10.
[13] Sheverdin A, Valagiannopoulos C. Core-shell nanospheres under visible light: optimal absorption, scattering, and cloaking. Phys Rev B 2019;99:075305.
[14] Gawande MB, Goswami A, Asefa T, et al. Core-shell nanoparticles: synthesis and applications in catalysis and electrocatalysis. Chem Soc Rev 2015;44:7540–90.
[15] Oulton RF. Surface plasmon lasers: sources of nanoscopic light. Rev Mater Today 2012;15(1–2):26–34.
[16] Premaratne M, Stockman M. Theory and technology of SPASERs. Rev Adv Opt Photon 2017;9(1):79–128.

[17] H-P S, Kryschi C. Facile design of a plasmonic nanolaser. Condens Matter 2017;2(1):8.
[18] Bergman DJ, Stockman MI. Surface plasmon amplification by stimulated emission of radiation: quantum generation of coherent surface plasmons in nanosystems. Phys Rev Lett 2003;90:027402.
[19] Stockman MI. Spaser action, loss compensation, and stability in plasmonic systems with gain. Phys Rev Lett 2011;106:156802.
[20] Noginov MA, Zhu G, Belgrave AM, et al. Demonstration of a spaser-based nanolaser. Nature 2009;460:1110–13.
[21] Gordon JA, Ziolkowski RW. The design and simulated performance of a coated nanoparticle laser. Opt Express 2007;15:2622–53.
[22] Gu P, DJS B, Chen Y. Dye-doped polystyrene-coated gold nanorods: towards wavelength tuneable SPASER. Methods Appl Fluoresc 2014;2:024004.
[23] Wang S, X-Y W, Li B, et al. Unusual scaling laws for plasmonic nanolasers beyond the diffraction limit. Nat Commun 2017;8:1889.
[24] Sikdar D, Rukhlenko ID, Cheng WL, Premaratne M. Tunable broadband optical responses of substrate-supported metal/dielectric/metal nanospheres. Plasmonics 2014;9:659–72.
[25] Motavas MH, Zarifkar A. Low threshold nanorod-based plasmonic nanolasers with optimized cavity length. Opt Laser Technol 2019;111:315–22.
[26] Mortensen NA. Nonlocal formalism for nanoplasmonics: phenomenological and semi-classical considerations. Photon Nanostruct 2013;11:303–16.
[27] Toscano G, Straubel J, Kwiatkowski A, et al. Resonance shifts and spill-out effects in self-consistent hydrodynamic nanoplasmonics. Nat Commun 2015;6:7132.
[28] Barbry M, Koval P, Marchesin F, Esteban R, et al. Atomistic near-field nanoplasmonics: reaching atomic-scale resolution in nanooptics. Nano Lett 2015;15:3410–19.
[29] Monreal RC, Antosiewicz TJ, Apell SP. Competition between surface screening and size quantization for surface plasmons in nanoparticles. N J Phys 2013;15:083044.
[30] Wubs M, Mortensen A. Nonlocal response in plasmonic nanostructures. In: Bozhevolnyi SI, Martin-Moreno L, Garcia-Vidal F, editors. Quantum plasmonics. Switzerland: Springer; 2017. p. 279–302.
[31] David C, de Abajo F J G. Spatial nonlocality in the optical response of metal nanoparticles. J Phys Chem C 2011;115:19470–5.
[32] McMahon JM, Gray SK, Schatz GC. Nonlocal optical response of metal nanostructures with arbitrary shape. Phys Rev Lett 2009;103:097403.
[33] Fernandez-Dominguez AI, Wiener A, García-Vidal FJ, et al. Transformation-optics description of nonlocal effects in plasmonic nanostructures. Phys Rev Lett 2012;108:106802.
[34] Derkachova A, Kolwas K, Demchenko I. Dielectric function for gold in plasmonics applications: size dependence of plasmon resonance frequencies and damping rates for nanospheres. Plasmonics 2016;11:941–51.
[35] Mortensen NA, Raza S, Wubs M, et al. A generalized non-local optical response theory for plasmonic nanostructures. Nat Commun 2014;5:3809.
[36] Tserkezis C, Stefanou N, Wubs M, Mortensen NA. Molecular fluorescence enhancement in plasmonic environments: exploring the role of nonlocal effects. Nanoscale 2016;8:17532–41.
[37] Kluczyk K, David C, Jacak WA. On quantum approach to modeling of plasmon photovoltaic effect. JOSA B 2017;34(10):2115–27.
[38] Cacciola A, Iatì MA, Saija R, et al. Spectral shift between the near-field and far-field optoplasmonic response in gold nanospheres, nanoshells, homo-and hetero-dimers. J Quant Spectr Radiat Trans 2017;195:97–106.
[39] Tserkezis C, Wubs M, Mortensen NA. Robustness of the rabi splitting under nonlocal corrections in plexcitonics. ACS Photon 2018;5(1):133–42.
[40] Sinha-Roy R, et al. Classical and ab initio plasmonics meet at sub-nanometric noble metal rods. ACS Photon 2017;4:1484–93.
[41] Kupresak M, Zheng X, GAE V, Moshchalkov VV. Comparison of hydrodynamic models for the electromagnetic nonlocal response of nanoparticles. Adv Theory Simul 2018:1800076.
[42] Rojas R, Claro F, Fuchs R. Nonlocal response of a small coated sphere. Phys Rev B 1988;37(12):6799–808.
[43] Huang Y, Gao L. Superscattering of light from core-shell nonlocal plasmonic nanoparticles. J Phys Chem C 2014;118(51):30170–8.
[44] Dong T. Investigation on plasmonic responses in multilayered nanospheres including asymmetry and spatial nonlocal effects. J Phys D 2017;50(49):495302.
[45] Eremina E, Eremin Y, Wriedt T. Computational nano-optic technology based on discrete sources method (review). J Mod Opt 2011;58(5–6):384–99.
[46] Yu E, Wriedt T. Analysis of the scattering properties of 3d non-spherical plasmonic nanoparticles accounting for non-local effects. J Mod Opt 2018;65(15):1778–86.
[47] Yu E, Doicu A, Wriedt T. Discrete sources method for modeling the nonlocal optical response of a nonspherical particle dimer. J Quant Spectr Radiat Trans 2018;217:35–44.
[48] Raza S, Bozhevolnyi SI, Wubs M, Mortensen NA. Nonlocal optical response in metallic nanostructures. Top Rev J Phys Condens Matter 2015;27:3204–300.
[49] Doicu A, Yu E, Wriedt T. Acoustic and electromagnetic scattering analysis using discrete sources. San Diego: Academic Press; 2000.
[50] Colton D, Kress R. Integral equation methods in scattering theory. New York: John Wiley & Sons; 1983.
[51] Mishchenko MI, Travis LD, Lacis AA. Scattering, absorption, and emission of light by small particles. Cambridge U. Press; 2002.
[52] Johnson PB, Christy RW. Optical constants of the noble metals. Phys Rev B 1972;6:4370–9.
[53] Meng X, Kildishev AV, Fujita K, et al. Wavelength-tunable spasing in the visible. Nano Lett 2013;13:4106–12.
[54] Viazmitinov DV, et al. Synthesis of core-shell Ag/SiO_2 nanoparticles for SPASER structures. J Phys 2014;541:012015.
[55] Avşar D, Ertürk H, Mengüç P. Plasmonic responses of metallic/dielectric core-shell nanoparticles on a dielectric substrate. Mater Res Express 2019;6:065006.